Permanent Magnets Aging in Variable Flux Permanent Magnet Synchronous Machines

Daniel Fernández[1], Maria Martinez[1], David Reigosa[1] Juan Guerrero[1], Carlos Suarez[2], Fernando Briz[1]
[1]Dept. of Elect., Computer & Systems Engineering
[2]Construction and Fabrication Engineering Department
University of Oviedo, Gijón, Spain
fernandezalodaniel@uniovi.es, martinezgmaria@uniovi.es, diazdavid@uniovi.es, guerrero@uniovi.es, csuarez@uniovi.es, fernando@isa.uniovi.es

***Abstract*— Permanent magnet synchronous machines (PMSMs) operation above base speed is typically achieved by injecting negative *d*-axis current to produce flux weakening. However, this mode of operation increases copper, stator/rotor core and permanent magnet (PM) losses, penalizing the efficiency and increasing the risk of demagnetization. Variable Flux PMSMs (VF-PMSM) in which PMs are magnetized/demagnetized during normal operation of the machine have been proposed to avoid the use of flux weakening current. However, PM aging due to magnetization/demagnetization cycles has not thoroughly studied yet. This paper analyzes the variation of NdFeB, SmCo and AlNiCo PMs properties, including magnetic, electric and thermal, resulting from magnetization/demagnetization cycles.[1]**

Keywords—Permanent magnet aging, remagnetization, variable flux permanent magnet synchronous machine.

I. Introduction

Operation of electric drives using PMSM, both interior PMSMs (IPMSMs) and surface PMSMs (SPMSMs) machines, can be especially challenging for applications in which the machine must operate at high speed, due to the need to inject negative current in the *d*-axis, also known as field weakening current [1]. Flux weakening current reduces the stator flux linkage, matching the back electromotive force (back-EMF) with the available voltage in the DC link. However, flux weakening current also increases the airgap flux harmonic content [2], [3], and consequently, eddy-currents in PMs, stator and rotor cores. This increases the losses and consequently the temperature of all machine elements [3].

To avoid the injection of flux weakening current and its subsequent adverse effects, variable flux PMSMs (VF-PMSM, also called memory motors) have been developed. In this type of machines, the PMs magnetization state (MS) is dynamically changed during high speed operation to reduce the needs of flux weakening current [4], [5].

[1]This work was supported in part by the Research, Technological Development and Innovation Programs of the Spanish Ministry Economy and Competitiveness, under grant MINECO-17-ENE2016-80047-R and by the Government of Asturias under project IDI/2018/000188 and FEDER funds.

VF-PMSMs can be equipped with different magnet types, including low coercivity (low-Hc) magnets like AlNiCo [6],[7] or SmCo [8], or a combination of low- and high-Hc magnets [3],[8]-[10]. VF-PMSMs equipping AlNiCo magnets require relatively small magnetic fields to change the MS [4], [6], [7]; this limits machine torque capability as the magnetic field produced by the *q*-axis current could demagnetize the PMs [8], [10]. VF-PMSMs combining low- and high-Hc magnets reduce the risk of undesired demagnetization due to *q*-axis current. In this configuration high-Hc magnets provide the base rotor magnetic field, which is unaffected by the stator current, while *d*-axis current pulses are used to changes the MS of low-Hc magnets. In all cases, VF-PMSMs low-Hc magnets must be magnetized/demagnetized as required by the working condition of the machine. VF-PMSMs magnetization is achieved in-situ by injecting a short current pulse from the stator terminals, i.e. the machine does not have to be disassembled [10]-[11]. VF-PMSMs MS can be manipulated thousands of times all along their life [6]. However, PMs aging produced by this repetitive process has not been analyzed yet.

Available literature on PMs aging effects focuses on PM properties variation due to temperature of operation [12]-[17] thermal cycling [18], [19] and annealing temperature profile during the sintering process [12]. In all studies, PM magnetic aging is divided into structure aging and magnetic aging. Structure aging is produced due to metallurgical changes, which modifies the magnetic domains with the consequent irrecoverable magnetic field strength loss [13]-[14]. Magnetic aging is a recoverable loss of magnetization, caused by the thermal agitation of magnetic domain walls [13]-[14]. PM suffering from magnetic aging can be reverted to their initial MS using a magnetizer.

This paper analyzes aging effects on PM magnetic, electric and thermal properties, due to magnetization /demagnetization cycles for PMs used in VF-PMSMs (i.e. NdFeB, SmCo and AlNiCo) [15]. The paper is organized as follows: characterization of PMs is discussed in section II, the experimental setup designed to cycle and characterize PMs is analyzed in Section III, experimental results using magnet samples are provided in Section IV, the effects of PMs aging in VF-PMSM is discussed in section V and the conclusions are finally provided in Section VI.

Table I. Typical magnetic, electric and thermal properties of different PMs.

Magnet Type	B_r (T)	α_B (%/K)	H_c (kA/m)	H_{cJ} (kA/m)	α_H (%/K)	BH_{max} kJ/m^3	ρ 10^{-6} (Ωm)	T_{max} (ºC)
Ferrite 27/25SH	0.400	-0.2	278	302	+0.3	30	104	250
AlNiCo Cast 80/12	1.11	-0.01~-0.035	130	126	-0.03~0.03	80	0.45-0.55	500
SmCo YXS24	1.02	-0.035	764	2000	-0.25	191	0.75-0.85	250
NdFeB N42SH	1.33	-0.11~-0.12	1018	1595	-0.56~-0.70	334	1.4-1.6	150

II. Characterization Of Permanent Magnets

This section describes the main magnetic, electric and thermal properties that characterize PM materials and that will be considered therefore for the study of PM aging:

- Magnetic properties. They can be obtained from the hysteresis loop, i.e. a plot of magnetic induction, B, and magnetic polarization, J, as a function of the magnetic field strength, *H*, (i.e. BH and JH curves) [20] as Fig. 1 shows. BH and JH curves provide the magnetic induction in the magnetic circuit and the flux density produced by the magnet alone vs. *H* respectively.
- Thermal properties. Can be evaluated from the analysis of the hysteresis loop at different temperatures [20].
- PM resistivity. This parameter will determine the magnet losses due to Eddy currents. PM resistivity can be estimated applying a time varying field to the PM [21].

Table I shows typical properties of four different PM types used in PMSMs: AlNiCo, ferrite, SmCo and NdFeB; where B_r is the magnet remanence and accounts the flux density of the magnet in a closed magnetic circuit without externally applied field, H_{cJ} is the intrinsic coercivity that measures the magnet's resistance to demagnetization, BH_{max} is the maximum energy product, i.e. a metric of the energy available for interaction within a magnetic circuit, ρ is the electrical resistivity, T_{max} is the maximum working temperature, α_B is the reversible thermal coefficient of B_r and α_H is the reversible thermal coefficient of H_{cJ}.

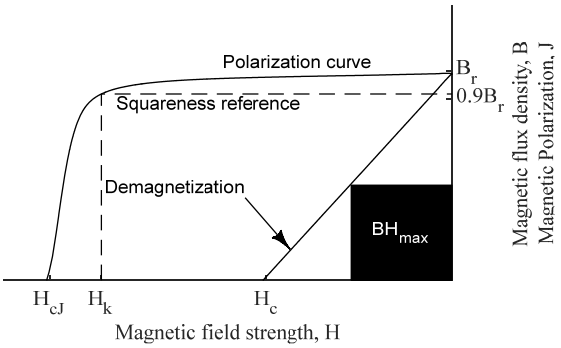

Fig. 1. Graphical representation of the magnetic parameters shown in Table I and the squareness factor.

Parameters listed in Table I, however, do not define the shape of the JH curve. A widely accepted metric to characterize the JH curve is the squareness factor (SF) in the second quadrant, also defined as squareness ratio (SR), (1), where $\mu_0 H_K$ is the knee field corresponding to a 10% magnetization loss, J, [22]. The squareness factor is representative of PM magnetic stability [22], i.e. the ability of the PM to preserve its magnetic properties irrespective of the applied external *H*.

$$SF = \frac{\mu_0 H_K}{\mu_0 H_{cJ}} \quad (1)$$

PM magnetic properties in Table I will be measured as described in IEC60404-05:2015 standard for closed magnetic circuits.

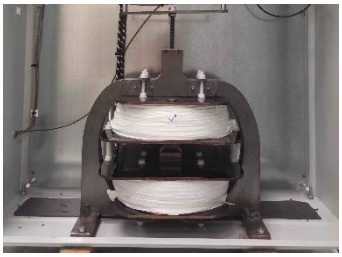

Fig. 2. Picture of the magnetizer yoke.

III. Experimental Setup

This section describes the experimental setup and further analysis used to study PMs aging effects and the methodology followed to emulate PM operating conditions in a VF-PMSM. An impulse magnetizer and a system to automatically change PM MS is proposed aiming to accelerate PM aging. PM magnetic properties variation due to aging are obtained using a hysteresisgraph.

A. Impulse Magnetizer

Fig. 2 shows the magnetizer yoke used for PM samples magnetization/ demagnetization, its main characteristics are given in Table II. The iron core is made of laminated soft magnetic material; its central column being movable to match PM sample size. Test samples have a cylindrical shape (see Fig. 3) with flat end faces. Fig. 4 shows the electric circuit used to control magnetic field strength applied. The capacitor bank "C" in Fig. 4 is first charged, and further discharged through coil "L" by turning on the IGBT (S_1) (see Fig. 4), the resulting field adjusted to modify the PM magnetization state as required. Contactor S_2 allows to reverse the field direction.

Table II: Peak magnetizer characteristics

Maximum voltage	720 V
Maximum energy	3500 J
Maximum airgap (With poles)	60 mm
Maximum airgap (without poles)	20 mm
Maximum field	2200 kA/m
Smaller side of the tapered pole, d_1 (see Fig. 6)	35 mm
Airgap length *l'* (see Fig. 3)	5 mm
Region with homogeneous field, d_2 (see Fig. 6)	27.5 mm

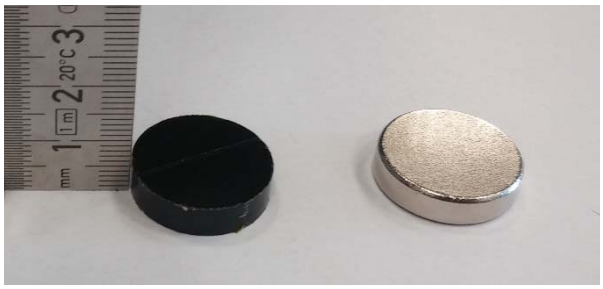

Fig. 3. NdFeB test samples, 20 mm diameter and 5 mm height with different coating

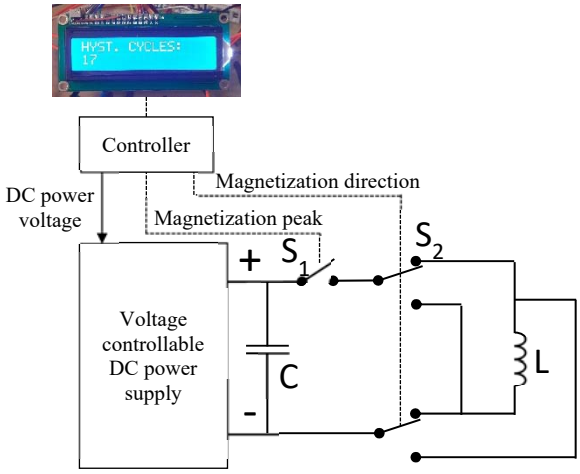

Fig. 4. Experimental setup for automatized magnetization/demagnetization.

Repeated magnetization/demagnetization of the magnet sample using the setup represented in Fig. 4, accelerates aging process in the PM sample.

B. Hyestresisgraph

The setup and procedure to obtain the hysteresis loop (i.e. BH curve) described following are specified by IEC 60404-5 standard. Fig. 5 shows the schematic representation of the setup.

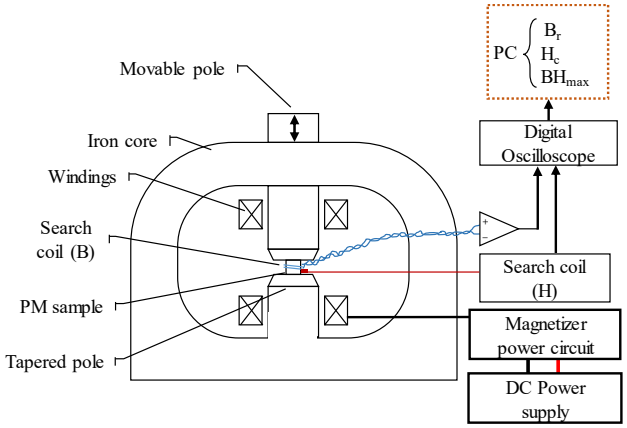

Fig. 5. Setup for BH curve measurement according to IEC 60404-5 standard.

Two search coils, see Figs. 5 and 6, are needed to measure the differential magnetic flux density (B), and the magnetic field strength (H). Initial magnetic remanence, Br, of each PM sample is obtained using a gauss meter. Coils are mounted on a plastic cylinder, its diameter being therefore constant and independent of PM samples diameter. PM test sample is surrounds by the *"B"* coil, its induced voltage being function of the flux passing through the PM test sample. *"H"* coil surrounds only support material (plastic). Since plastic is a paramagnetic material, it will not saturate, therefore the induced voltage in *"H"* coil will provide the information of the total magnetic field strength applied by the magnetizer. Fig. 7a and 7c shows the induced voltages in the two search coils during a remagnetization process; Fig. 7b and 7d showing the resulting magnetic flux obtained in each coil. Changes in the PM magnetic flux density, ΔB (2), are obtained by integrating the voltage induced in *"B"* coil, U_B (see Fig. 7a and 7c), where B_2 and B_1 are the magnetic flux densities in the instant t_2 and t_1 respectively, A_B is the cross-section area of the PM sample and N_B is the number of turns of the *"B"* search coil. The total magnetic field strength, H (3), is obtained by integrating the voltage induced in *"H"* coil, U_H, (see Fig. 7b and 7d), where H_2 and H_1 are the magnetic field strength in the instant t_2 and t_1 respectively, A_H is the cross-section area of the plastic support and N_H is the number of turns of the *"H"* coil. *"H"* coil must be placed within a homogeneous field in the airgap close to the PM sample, according to IEC60404-05 and the test sample and coil axes must be aligned. The dimensions of the region with homogeneous field are given by (4) and (5), where d_1 is the dimension of the smallest side of a rectangular pole piece, d_2 is the maximum diameter of the cylindrical volume with a homogeneous field and l' is the distance between the pole pieces, see Fig. 6b. Dimensions d_1, d_2 and l' for the tapered poles and PM sample size are listed in Table II.

Fig. 7e shows flux induced in *"B"* coil vs. flux induced in *"H"* coil during the remagnetization process shown in Fig. 7 a-d. The demagnetization curve of the PM is usually represented as B-H or J-H, J being the polarization, obtained from (6).

$$\Delta B(t) = B_2(t) - B_1(t) = \frac{1}{A_B N_B}\int_{t_1}^{t_2} U_B(t)dt \qquad (2)$$

$$\Delta H(t) = H_2(t) - H_1(t) = \frac{1}{\mu_0 A_H N_H}\int_{t_1}^{t_2} U_H(t)dt \qquad (3)$$

$$d_1 \geq d_2 + 1.2l' \qquad (4)$$

$$d_1 \geq 2.0l' \qquad (5)$$

$$J = B - \mu_0 H \qquad (6)$$

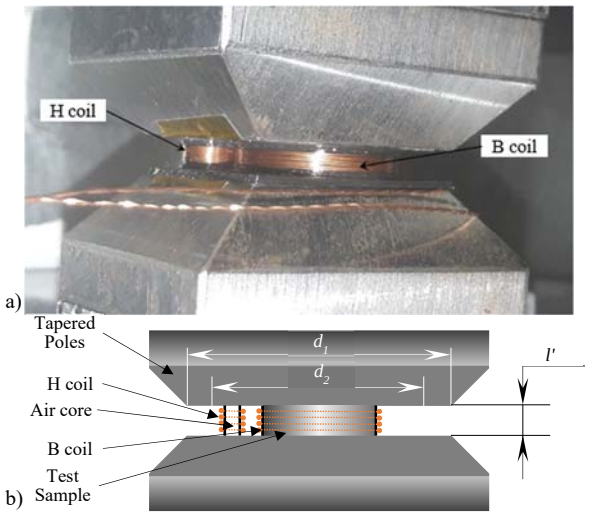

Fig. 6. Search coils for H and B measurements, a), real system, and b), schematic representation of the cross section

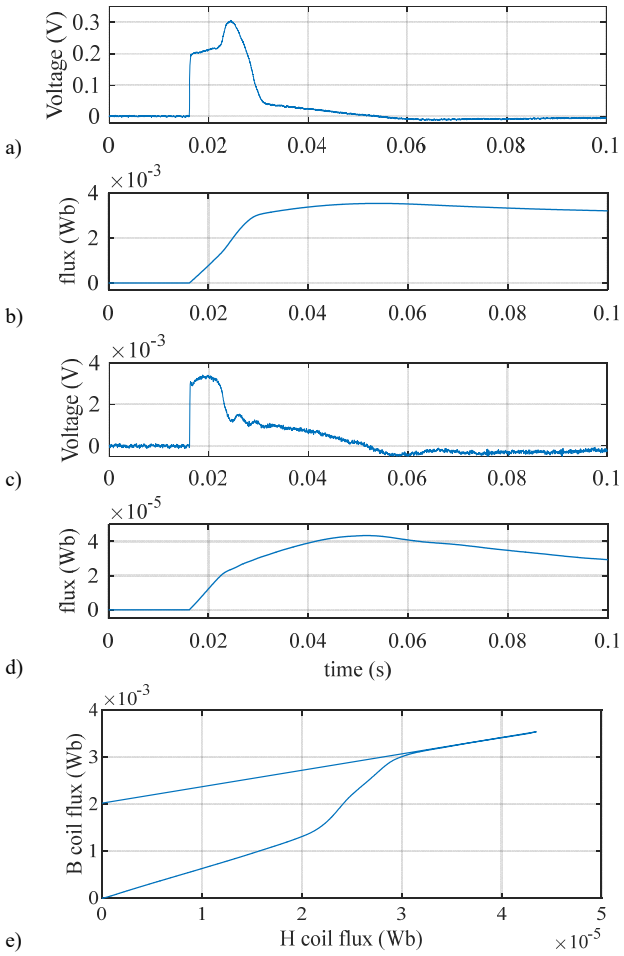

Fig. 7. Induced voltage in "B" coil, a), and resulting flux in "B" coil, b), induced voltage in "H" coil, c), resulting flux in "H" coil, d), and B coil flux vs. H coil flux, e), during a remagnetization process.

C. *PM resistivity estimation*

PM resistivity can be also a metric of the PM aging. PM magnet resistance is estimated from the induced eddy currents in the magnet due to an externally applied time varying magnetic field [21],[23], the frequency must be chosen to avoid skin effect and full penetration of the high frequency magnetic field in the PM material. The system shown in Fig. 8 has been used for this purpose [21],[23] the signal injected is varied from 0.1 to 1kHz; the upper limit being chosen considering he skin depth of the PM.

It consists of an iron powder core, to minimize eddy current losses, a coil and an adjustable airgap to fit the PM size. The coil is fed from an H-bridge converter able to inject a high frequency signal of different frequencies and amplitudes into the coil, which will be used to induce a high frequency flux through the PM. The resulting high frequency Eddy currents in the PM will depend on its resistivity. The PM resistivity will be estimated from the coil voltages and currents [21],[23].

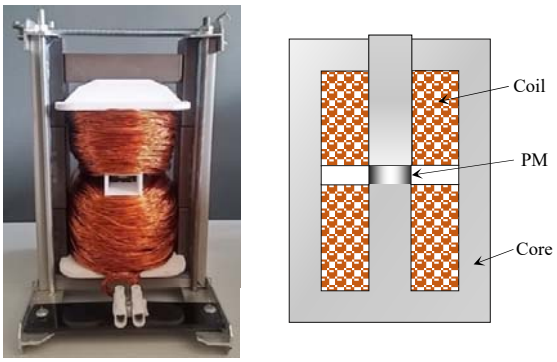

Fig. 8. Experimental setup used for PM high frequency resistance evaluation

IV. EXPERIMENTAL RESULTS

Experimental results using PMs samples shown in Fig. 3 have been conducted. PM samples materials (see Table III) are from two different manufacturers and include high-Hc (NdFeB) PMs and low-Hc magnets (SmCo and AlNiCo).

Table III. Classification of evaluated PM samples

PM	Class	Manufacturer	Cost
NdFeB_1	N42SH	A	Low
NdFeB_2	N42SH	B	High
SmCo	YXS24	A	Low
AlNiCo	CAST 80/12	A	High

A. *Test conditions*

MS changes occurring in actual VF-PMSMs will obviously depend on the road characteristics and the driving style and obviously it is not possible to reproduce them precisely. For the experimental results shown in this section a simplified driving profile has been defined, it is shown in Fig. 9a. PMs are initially fully magnetized starting BH curve begin measured under these conditions. MS is further varied repeatedly between 50% and 85% as shown in Figs. 9a and b. The power supply in Fig. 4 operates with variable voltage, the cadency of demagnetization/remagnetization pulses has been adjusted to keep the magnetizer coils at a safe temperature of 30ºC. The driving cycle is repeated several times, every driving cycle containing one thousand of magnetization/remagnetization cycles. Once the test is finished, the PM is fully magnetized, the BH curve being obtained as required by standard IEC60404-05:2015.

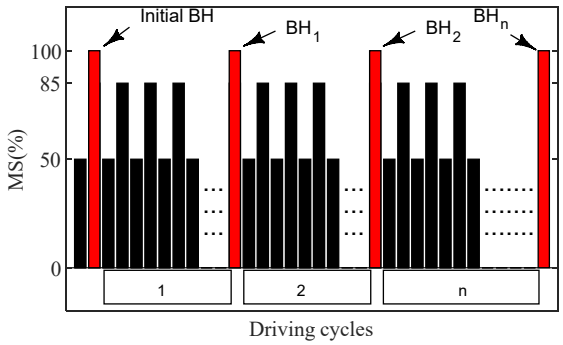

a)

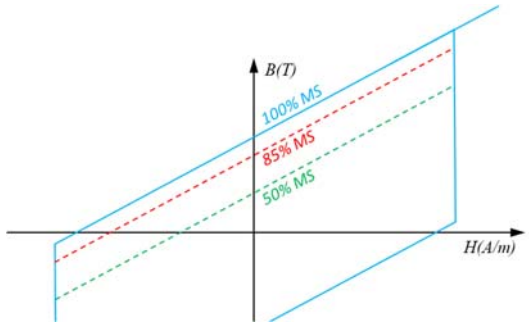

b)

Fig. 9. PM MS changes a) during the driving cycle used in the experiments and b) representation in the BH curve.

B. Effects of cycling on PM magnetic properties

Fig. 10 shows the demagnetization curve of the sample NdFeB_1 at the beginning of the cycling process, i.e. 0 cycles, and after 2k, 4k and 5k driving cycles. It can be observed that both B-H and J-H curves decrease with cycling. Table IV shows the changes in the main properties of the magnet with cycling, all of them are seen to get worse. Fig. 11 shows same results as Fig. 10 for sample NdFeB_2. This sample was supplied by a different manufacturer, it has a relatively higher cost and, and is expected to have superior characteristics. Variation of magnetic properties of NdFeB_2 samples are summarized in Table V. While the degradation is in general less relevant than for sample NdFeB_1, aging effects are still evident, the highest impact of being observed again in the maximum energy product, BHmax.

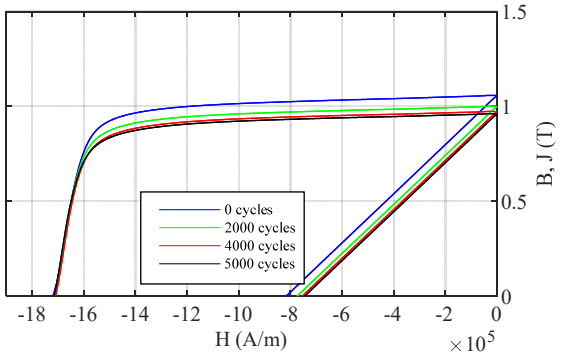

Fig. 10. BH curve of sample NdFeB_1 for 0, 2000, 4000 and 5000 cycles. Constant PM temperature, 30ºC.

Table IV: PM Properties variation of NdFeB_1 sample (Fig. 10)

	0 cycles	5k cycles	Variation
B_r (T)	1.056	0.9591	- 11%
BH_{max} (kJ/m^3)	215	178	- 20.7%
H_c (kA/m)	-814	-742	- 9.7%
H_{cJ} (kA/m)	-1714	-1708	- 0.3%
SF	0.843	0,838	-0.5%
Estimated HF resistance (Ω) @250Hz	0.832	0.874	+ 5.1%

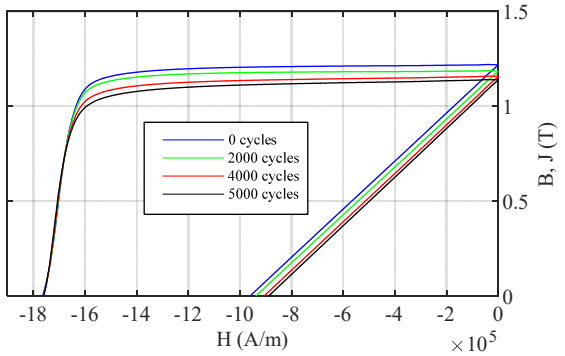

Fig. 11. BH curve of sample NdFeB_2, same conditions as for Fig. 10.

Fig. 12 and Table VI shown the results when SmCo samples are subjected to the cycling process. It can be observed that both B-H and J-H curves have been slightly affected, the most noticeable changes occurring in the maximum energy product; on the other hand, practically no effect is observed in the estimated high frequency resistance.

Table V: PM Properties variation of NdFeB_2 sample (Fig. 11)

	0 cycles	5k cycles	Variation
B_r (T)	1.216	1.136	- 7%
BH_{max} (kJ/m^3)	292	252	- 15%
H_c (kA/m)	-954	-885	- 7.7%
H_{cJ} (kA/m)	-1763	-1758	- 0.2%
SF	0.905	0,891	-1.5%
Estimated HF resistance (Ω) @250Hz	0.892	0.948	+ 6.3%

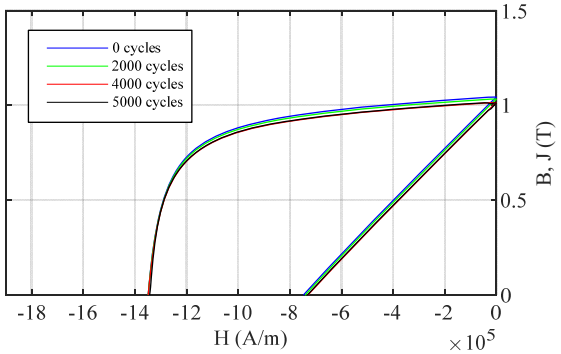

Fig. 12. BH curve of sample Sm2Co17 for 0, 2000, 4000 and 5000 cycles. Constant PM temperature, 30ºC.

Table VI: PM Properties variation of SmCo sample

	0 cycles	5k cycles	Variation
B_r (T)	1.044	1.014	- 2,9%
BH_{max} (kJ/m^3)	199	190	- 4.7%
H_c (kA/m)	-740	-721	- 2.6%
H_{cJ} (kA/m)	-1348	-1342	- 0.4%
SF	0.603	0,615	+2%
Estimated HF resistance (Ω) @250Hz	0.176	0.176	+ 0%

Finally, Fig. 13 and Table VII show the results for AlNiCo samples. It can be observed that the degradation in this case has different characteristics. B_r is seen to suffer the

highest impact, while H_c remains almost constant; also AlNiCo is the only material showing relevant variations of H_{cJ}.

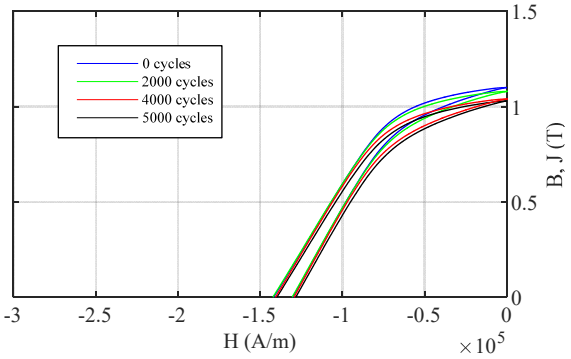

Fig. 13. BH curve of sample AlNiCo for 0, 2000, 4000 and 5000 cycles. Constant PM temperature, 30ºC.

Table VII: PM Properties variation of AlNiCo sample

	0 cycles	5k cycles	Variation
B_r (T)	1.099	1.030	- 6.6%
BH_{max} (kJ/m^3)	76	73	- 4.1%
H_c (kA/m)	-130.4	-129.6	- 0.6%
H_{cJ} (kA/m)	-142.3	-139.6	- 2.0%
SF	0,41	0,40	-2.5%
Estimated HF resistance (Ω) @250Hz	0.577	0.593	+ 2.7%

Fig. 14 shows a comparison of the relative PM remanence variation in a closed magnetic circuit vs. number of remagnetization cycles. It can be observed from the figure that PM remanence remains rather stable for all PM samples when the number of cycles is <500. For higher cycles counts all PM samples experiment a remanence drop, the effect begin more relevant in NdFeB PMs. On the contrary, SmCo sample shows the lowest sensitivity. In all cases a peak magnetization field of ≈3.34T is applied, which is the limit of the magnetizer. Following the pulse PM magnetic properties (i.e. BH and JH curves) stare measured.

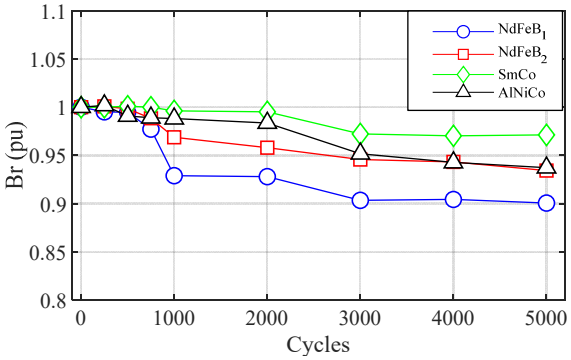

Fig. 14. PM remanence measured for different PM samples for different number of magnetization/demagnetization cycles. Constant PM temperature, 30ºC.

Aging in permanent magnets could be due to several reasons, e.g. magnetostriction and coating. Magnetostriction is the change in shape of crystal of ferromagnetic materials subject to an external magnetic field due to changes in the orientation (rotation) of the small magnetic domains. On the other hand, NdFeB magnets used in the experiments as well as AlNiCo magnets were coated using a NiCuNi structure. Coated magnets show a reduced magnetization capability [27], coating can also affect to PM magnet electromagnetic behavior [27], [28]. Precise understanding of this phenomena is a subject of ongoing research.

C. Effects of cycling on PM thermal coefficient of remanence α_B

Effects of cycling on thermal coefficient of remanence is analyzed in this section. To perform this analysis, SmCo and AlNiCo magnets should be operated at a temperature of >250 ºC, and NdFeB magnets at a temperature ≈120 ºC. Unfortunately, the experimental setup currently available is unable to reach the temperatures required for the analysis of SmCo and AlNiCo magnets. Consequently, the analysis presented in this section has been restricted to NdFeB magnets.

Fig. 15a shows the PM flux measured in an open magnetic circuit for different PM temperatures. PM flux is decreased with the number of cycles, which is consistent with the results shown in Fig. 10. It is also observed from Fig. 15a that the knee point, which corresponds to the maximum working temperature, does not change with cycling. Fig. 15b shows the flux density difference between the non-cycled and the cycled PM vs. magnet temperature; it is observed a slight increase in the reversible thermal coefficient of remanence, α_B , due to the cycling process, i.e. $slope \neq 0$, which means that PM flux temperature dependence change when the sample has been cycled.

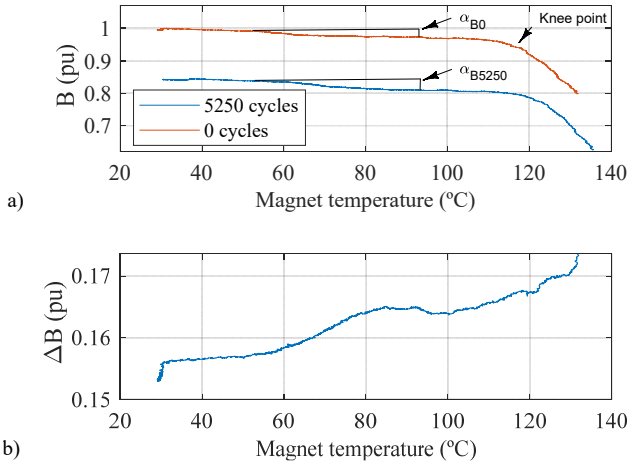

Fig. 15. PM flux variation with temperature (open circuit) and b) PM flux difference between non-cycled and cycled PM (curves in Fig. 15a).

It is finally noted that upgrading the experimental setup to allow evaluation of the thermal behavior of SmCo and AlNiCo is currently being studied, but presents remarkable challenges.

D. Effects of cycling on PM high frequency resistance

Knowledge of the effect of cycling on the magnet resistance is relevant, as this will affect to the magnet losses

due to Eddy currents [25]. Direct measurement of magnet resistance in NdFeB PMs is not reliable due the NiCuNi coating being applied. PM high frequency resistance has been estimated instead using the system shown in Fig. 8, the results for each type of magnet are included in Tables IV to VII. The increase of the estimated PM HF resistance is consistent with the results shown in Figs. 10 to 14, as PM high frequency resistance is a reliable indicator of the PM MS [23]. NdFeB magnets show the largest high frequency resistance variation with cycling, followed by AlNiCo magnets. On the contrary, SmCo magnets are barely affected.

E. Effects of cycling on PM flux distribution

Non-uniform flux distributions in the PM will result in airgap flux harmonic components due to the machine magnetomotive force (MMF), eventually increasing core losses and torque ripple, therefore penalizing machine efficiency and performance [4]. PM surface flux density distribution was measured for the case of uncycled and cycled PMs in an open magnetic circuit using a Gauss meter. Fig 16a shows the magnetic flux density measured all along the diameter (*D*) (see Fig. 17), of the PM sample NdFeB_2 before and after cycling, the adverse impact of cycling on PM magnetic flux density distribution being evident from the figure. Since the only difference between the PM samples used to obtain the results shown in Fig. 16a was the cycling process, PM flux density variation, see Fig. 16b, is expected to be due to the aging phenomena.

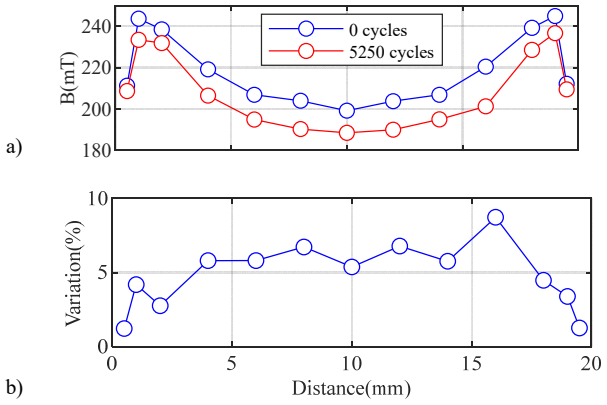

Fig. 16. PM flux density distribution open circuit measurement on PM surface for the sample NdFeB_2, a) before and after 5250 cycles, b) PM flux density variation

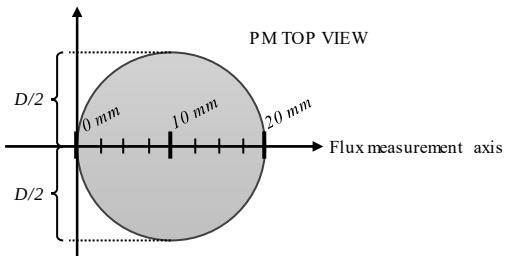

Fig. 17. Displacement line of the Gauss-meter on the PM sample surface.

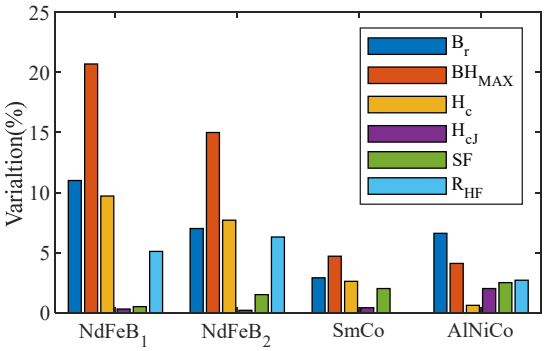

Fig. 18. PM properties variation (absolute) due to cycling for the results listed in Table IV to Table VII.

Fig. 18 shows a summarizes the results shown in this section. It is concluded that SmCo and AlNiCo magnets shows the lower sensitivity compared to NdFeB magnets.

V. Effects Of PM Aging On VF-PMSMs

All the previous analyses have focused on discrete magnets. Maximum torque reduction, losses increase, increased risk of PM irreversible demagnetization and efficiency reduction will be direct consequences of PM aging in VF-PMSMs.

Preliminary analysis of the effects of PM degradation on VF-PMSM due to cycling has been addressed by means of FEA for a VF-PMSM using NdFeB magnets. Main parameters are shown in Table VIII. VF-PMSM properties variation due to aging are shown Table IX.

Table VIII: Machine parameters of the VF-PMSM

Parameter	Value	Units
Peak Power	93	kW
Peak Torque	277	Nm
Magnet type	N-42SH (NdFeB)	
Outer diameter	198	Mm
Stack length	150	Mm

Total torque generated by a PMSM is (7) where p is the number of pole pairs of the machine, λ_{PM} is the PM flux linkage, i_{ds} and i_{qs} are the direct and quadrature axes currents respectively and L_d and L_q are the direct and quadrature axes inductances respectively; the first term of (7) is commonly known as electromagnetic torque (T_e) the second on as reluctance torque ($T_{\Re}$).

$$T = \frac{3p}{2}(\lambda_{PM} i_{qs} + (L_d - L_q) i_{ds} i_{qs}) = T_e + T_{\Re} \qquad (7)$$

When a PM has been cycled its flux density is weaker, affecting to both electromagnetic and reluctance torques. Fig. 19 shows the demagnetization curves before and after cycling the sample NdFeB_2 for the ideal load line, where the working point changes from operating point OP_1 to OP_2. Taking into account that for a given load line there is a linear relationship between PM remanence B_r and flux linkage λ_{PM}, the electromagnetic torque, T_e (7), will be therefore reduced. On the other hand L_d in IPMSMs tends to be particularly sensitive the magnetic saturation level of the machine [26]; therefore if B_r decreases, L_d will increase, resulting in a reduction of reluctance torque $T_{\Re}$, see Table IX.

To maintain the torque level, it is possible to compensate the flux reduction by an increase of the current, but of course this will increase the risk of demagnetization and a lower limit of the machine overload capability.

Table IX: Machine parameters of the VF-PMSM

Parameter	Before aging	After aging	Variation (%)
Peak Torque (Nm)	277.8	253.4	-9.4%
Peak Power (W)	92.9	87.8	-7.4%
Efficiency @ peak power (%)	93.9	90.51	-3.6%
PM losses @ peak power (W)	223	231	+2.9 %
Ld @ no load (μH)	126	130	+3.1%
Lq @ no load (μH)	352	355	+0.85%

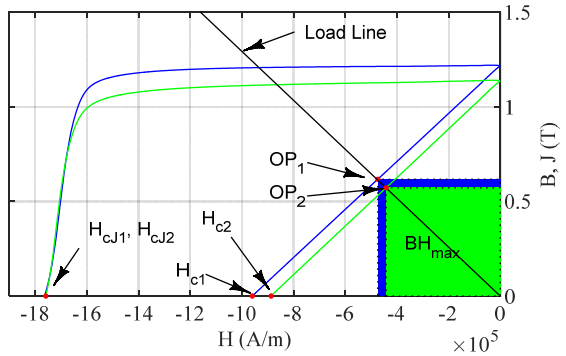

Fig. 19. PM remanence measured for different PM samples for differnt number of remagnetization cycles. Constant PM temperature, 30ºC.

Variations of L_d can also affect the controllability of the machine; *d*-axis current regulator is highly dependent on machine parameters and therefore, variations of L_d can affect its dynamics, including time response or even compromising its stability. The consequences of a non-uniform magnetic flux density distribution in a VF-PMSM are additional harmonic components in the MMF waveform. This will lead to higher core losses and lower machine performance.

VI. Conclusions

Aging effects of the PM used in VF-PMSM (i.e. NdFeB, SmCo and AlNiCo) due to magnetization/demagnetization cycles have been analyzed in this paper. It has been shown that cycling has a direct impact on PM magnetic, electrical and thermal properties. Changes of B-H and J-H curves with cycling has been evaluated, it has been concluded that cycled magnets have lower magnetic energy, remanence and coercivity. It has also been shown that cycling increases the thermal remanence coefficient of the magnet. All these effects contribute to reduce the torque capability and efficiency of VF-PMSMs. The estimated PM high frequency resistance is seen to be also increased with cycling, which results in higher PM losses, higher demagnetization risk and in a reduction of the machine efficiency. Finally, it was shown that aging of PMs due to demagnetization/magnetization processes results in a non-uniform magnetic field distribution, which in PMSMs may make the MMF waveform to change, resulting therefore in a variation of the airgap flux harmonic content, which could have a negative impact on the machine losses.

References

[1] T. M. Jahns, "Flux-Weakening Regime Operation of an Interior Permanent-Magnet Synchronous Motor Drive," in *IEEE Transactions on Industry Applications*, vol. IA-23, no. 4, pp. 681-689, July 1987.doi: 10.1109/TIA.1987.4504966

[2] Jang-Mok Kim and Seung-Ki Sul, "Speed control of interior permanent magnet synchronous motor drive for the flux weakening operation," in *IEEE Transactions on Industry Applications*, vol. 33, no. 1, pp. 43-48, Jan.-Feb. 1997.doi: 10.1109/28.567075

[3] K. Sakai, K. Yuki, Y. Hashiba, N. Takahashi and K. Yasui, "Principle of the variable-magnetic-force memory motor," *IEEE ICEMS*, pp. 1-6, Tokyo, 2009. doi: 10.1109/ICEMS.2009.5382812

[4] Z. Q. Zhu, Y. S. Chen and D. Howe, "Iron loss in permanent-magnet brushless AC machines under maximum torque per ampere and flux weakening control," *IEEE Trans. on Mag.*, vol. 38, no. 5, pp. 3285-3287, Sep 2002. doi: 10.1109/TMAG.2002.802296

[5] V. Ostovic, "Memory motors-a new class of controllable flux PM machines for a true wide speed operation," *IEEE Industry Applications Conference (IAS)*, vol.4, pp. 2577-2584, Chicago, IL, USA, 2001. doi: 10.1109/IAS.2001.955983

[6] V. Ostovic, "Memory motors," *IEEE Industry Applications Magazine*, vol. 9, no. 1, pp. 52-61, Jan/Feb 2003. doi: 10.1109/MIA.2003.1176459

[7] M. Ibrahim, L. Masisi and P. Pillay, "Design of Variable-Flux Permanent-Magnet Machines Using Alnico Magnets," in *IEEE Transactions on Industry Applications*, vol. 51, no. 6, pp. 4482-4491, Nov.-Dec. 2015. doi: 10.1109/TIA.2015.2461621

[8] A. Sun, J. Li, R. Qu, J. Chen and H. Lu, "Rotor design considerations for a variable-flux flux-intensifying interior permanent magnet machine with improved torque quality and reduced magnetization current," *2015 IEEE Energy Conversion Congress and Exposition (ECCE)*, Montreal, QC, 2015, pp. 784-790. doi: 10.1109/ECCE.2015.7309769

[9] H. Liu, H. Lin, S. Fang and Z. Q. Zhu, "Permanent Magnet Demagnetization Physics of a Variable Flux Memory Motor," *IEEE Trans. on Mag.*, vol. 45, no. 10, pp. 4736-4739, Oct. 2009. doi: 10.1109/TMAG.2009.2021408

[10] A. Athavale, K. Sasaki, B. S. Gagas, T. Kato and R. D. Lorenz, "Variable Flux Permanent Magnet Synchronous Machine (VF-PMSM) Design Methodologies to Meet Electric Vehicle Traction Requirements with Reduced Losses," in *IEEE Transactions on Industry Applications*, vol. 53, no. 5, pp. 4318-4326, Sept.-Oct. 2017. doi: 10.1109/TIA.2017.2701340

[11] H. Hua, Z. Q. Zhu, A. Pride, R. P. Deodhar and T. Sasaki, "A Novel Variable Flux Memory Machine With Series Hybrid Magnets," in *IEEE Transactions on Industry Applications*, vol. 53, no. 5, pp. 4396-4405, Sept.-Oct. 2017.doi: 10.1109/TIA.2017.2709261

[12] D. Eckert, K. -. Muller, M. Wolf, W. Rodewald and B. Wall, "Ageing effects in sintered (Nd,Dy)/sub 15/(Fe,Co,Mo,Al)/sub 77/B/sub 8/ permanent magnets," in *IEEE Transactions on Magnetics*, vol. 29, no. 6, pp. 2755-2757, Nov. 1993. doi: 10.1109/20.280922

[13] Niedra, J., "M-H Characteristics and Demagnetization Resistance of Samarium-Cobalt Permanent Magnets to 300 C," NASA Contract report 189194, Aug. 1992, doi:10.4271/929263.

[14] J. Niedra and E. Overton, " 23 to 300 °C Demagnetization Resistance of Samarium-Cobalt Permanent Magnets," NASA Technical Paper 3119, Nov. 1991.

[15] D. Fernández, M. Martinez, D. Reigosa, J. Guerrero, C. Suarez and F. Briz, "Permanent Magnets Aging in Variable Flux Permanent Magnet Synchronous Machines," *2018 IEEE Energy Conversion Congress and Exposition (ECCE)*, Portland, OR, 2018, pp. 236-241. doi: 10.1109/ECCE.2018.8558075

[16] M. Haavisto, H. Kankaanpaa and M. Paju, "Estimation of Time-Dependent Polarization Losses in Sintered Nd-Fe-B Permanent Magnets," in *IEEE Transactions on Magnetics*, vol. 47, no. 1, pp. 170-174, Jan. 2011.doi: 10.1109/TMAG.2010.2089692

[17] M. Haavisto, S. Tuominen, H. Kankaanpaa and M. Paju, "Time Dependence of Demagnetization and Flux Losses Occurring in Sintered Nd-Fe-B Permanent Magnets," in *IEEE Transactions on*

Magnetics, vol. 46, no. 9, pp. 3582-3584, Sept. 2010. doi: 10.1109/TMAG.2010.2047262

[18] Minna Haavisto, Sampo Tuominen, Timo Santa-Nokki, Harri Kankaanpää, Martti Paju, and Pekka Ruuskanen, "Magnetic Behavior of Sintered NdFeB Magnets on a Long-Term Timescale," Advances in Materials Science and Engineering, vol. 2014, 7 pages, Article ID 760584, 2014. doi:10.1155/2014/760584

[19] D. Huger and D. Gerling, "The effects of thermal cycling on aging of Neodymium-Iron-Boron magnets," *IEEE International Conference on Power Electronics and Drive Systems*, pp. 389-392, Sydney, 2015. doi: 10.1109/PEDS.2015.7203464

[20] F. Fiorillo, "Characterization and Measurement of Magnetic Materials", Elsevier Academic Press, 1st Edition. 7th December 2004, eBook ISBN: 9780080528922,

[21] D. Fernandez, D. D. Reigosa, J. M. Guerrero, Z. Zhu and F. Briz, "Permanent-Magnet Magnetization State Estimation Using High-Frequency Signal Injection," in *IEEE Transactions on Industry Applications*, vol. 52, no. 4, pp. 2930-2940, July-Aug. 2016.doi: 10.1109/TIA.2016.2541616

[22] E. A. Perigo, H. Takiishi, C. C. Motta and R. N. Faria, "On the Squareness Factor Behavior of RE-FeB (RE $=$ Nd or Pr) Magnets Above Room Temperature," in *IEEE Transactions on Magnetics*, vol. 45, no. 10, pp. 4431-4434, Oct. 2009.doi: 10.1109/TMAG.2009.2025190

[23] D. Díaz Reigosa, D. Fernandez, Z. Zhu and F. Briz, "PMSM Magnetization State Estimation Based on Stator-Reflected PM Resistance Using High-Frequency Signal Injection," in *IEEE Transactions on Industry Applications*, vol. 51, no. 5, pp. 3800-3810, Sept.-Oct. 2015.doi: 10.1109/TIA.2015.2437975

[24] T. Fukushige, N. Limsuwan, T. Kato, K. Akatsu and R. D. Lorenz, "Efficiency Contours and Loss Minimization Over a Driving Cycle of a Variable Flux-Intensifying Machine," in *IEEE Transactions on Industry Applications*, vol. 51, no. 4, pp. 2984-2989, July-Aug. 2015. doi: 10.1109/TIA.2015.2404918

[25] D. Fernández, M. Martínez, D. Reigosa, J. M. Guerrero, C. M. Suárez Alvarez and F. Briz, "Impact of Machine Magnetization State on Permanent Magnet Losses in Permanent Magnet Synchronous Machines," in *IEEE Transactions on Industry Applications*, vol. 55, no. 1, pp. 344-353, Jan.-Feb. 2019.doi: 10.1109/TIA.2018.2867326

[26] N. Bianchi, T. M. Jahns, "Design, Analysis ans Control of Interior Permanent Magnet Synchronous Machines," Tutorial Course Notes, pp. 2.5-2.6, October 2004.

[27] D. Fernandez, D. Reigosa, J. M. Guerrero, Z. Q. Zhu, C. Suarez and F. Briz, "Influence of PM Coating on PM Magnetization State Estimation Methods Based on Magnetoresistive Effect," in *IEEE Transactions on Industry Applications*, vol. 54, no. 3, pp. 2141-2150, May-June 2018. doi: 10.1109/TIA.2018.2797883

[28] Liu, Yapi, " Discussion On Several Principal Problems Aroused From Measuring High Performance Permanent Magnetic Materials," in *International Journal of Applied Electromagnetics and Mechanics*, vol. 55, no. 3, pp. 453-479, Oct. 2017.